All Inorganic Cesium Lead Iodide Perovskite Nanowires with Stabilized Cubic Phase at Room Temperature and Nanowire Array-Based Photodetectors

Aashir Waleed,[†] Mohammad Mahdi Tavakoli,[†,‡] Leilei Gu,[†] Shabeeb Hussain,[†,§] Daquan Zhang,[†] Swapnadeep Poddar,[†] Ziyi Wang,[⊥] Rongjun Zhang,[⊥] and Zhiyong Fan[*,†]

[†]Department of Electronic and Computer Engineering, The Hong Kong University of Science and Technology, Clear Water Bay, Kowloon, Hong Kong SAR, China

[‡]Department of Materials Science and Engineering, Sharif University of Technology, 113659466, Azadi Avenue, Tehran, Iran

[§]Catalysis and Nanomaterials Lab 27, Department of Chemistry, Quaid-i-Azam University, Islamabad 45320, Pakistan

[⊥]Department of Optical Science and Engineering, Fudan University, Shanghai 200433, China

S Supporting Information

ABSTRACT: Alluring optical and electronic properties have made organometallic halide perovskites attractive candidates for optoelectronics. Among all perovskite materials, inorganic $CsPbX_3$ (X is halide) in black cubic phase has triggered enormous attention recently owing to its comparable photovoltaic performance and high stability as compared to organic and hybrid perovskites. However, cubic phase stabilization at room temperature for $CsPbI_3$ still survives as a challenge. Herein we report all inorganic three-dimensional vertical $CsPbI_3$ perovskite nanowires (NWs) synthesized inside anodic alumina membrane (AAM) by chemical vapor deposition (CVD) method. It was discovered that the as-grown NWs have stable cubic phase at room temperature. This significant improvement on phase stability can be attributed to the effective encapsulation of NWs by AAM and large specific area of these NWs. To demonstrate device application of these NWs, photodetectors based on these high density $CsPbI_3$ NWs were fabricated demonstrating decent performance. Our discovery suggests a novel and practical approach to stabilize the cubic phase of $CsPbI_3$ material, which will have broad applications for optoelectronics in the visible wavelength range.

KEYWORDS: Perovskite, cesium lead iodide, nanowires, stability, anodic alumina membrane, photodetector
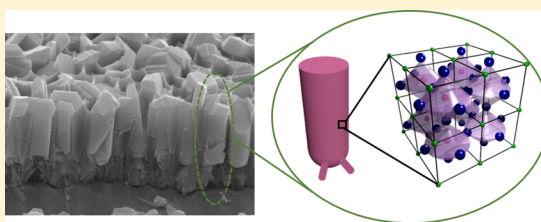
Hybrid organic inorganic perovskites with formula ABX_3 (A = organic cation, B = metal, X = halide) have triggered enormous attention due to their alluring optical and electronic properties including high optical absorption, long carrier diffusion length, and high carrier mobility.[1−5] These properties make them highly promising materials for high-performance optoelectronic devices such as solar cells,[6,7] photodetectors, and light-emitting diodes (LEDs).[8−10] However, organic-based perovskites suffer from their poor ambient stability in humid air,[11,12] which hinders their practical applications. As a result, it has attracted a great deal of attention to replace the organic component in the hybrid perovskite material with inorganic elements to address the stability issue. Recently, cesium lead iodide perovskite ($CsPbI_3$) was found to have high stability with excellent physical properties, which can be harnessed for fabrication of high-performance optoelectronic devices.[13−18] Intriguingly, it has been discovered that the black cubic phase $CsPbI_3$ with a band gap of 1.74 eV is particularly useful for various optoelectronic applications. Unfortunately, it was also found that $CsPbI_3$ perovskite has two phases, namely cubic phase and orthorhombic phase, and the preferred black cubic phase quickly undergoes phase transformation to orthorhombic phase

after fabrication at room temperature.[19,20] Therefore, cubic phase stabilization is a bottleneck challenge in realization of devices based on $CsPbI_3$. Up-to-date, there have been a few attempts to stabilize cubic phase of $CsPbI_3$ thin films at room temperature by tuning chemical composition, including hydro-iodic acid (HI), solvent engineering using isopropyl alcohol (IPA), and composition alteration with Cl halide.[15,21,22] All the reported methods are solution-based process and have common principle of chemical composition alteration which causes shifting in absorbance peak. Interestingly, it was discovered later that phase stability can be further enhanced by reducing the grain size of $CspbI_3$ film, which increases surface energy as compared to large grains.[23,24] Also, Swarnkar et al. shows that nanocolloidal $CsPbI_3$ with cubic phase is stable at room temperature due to nanoscale confinement and effective removal of excess precursor from growth solution.[24]

In this work, we have discovered that high density vertical arrays of $CsPbI_3$ (NWs) with room-temperature stable cubic
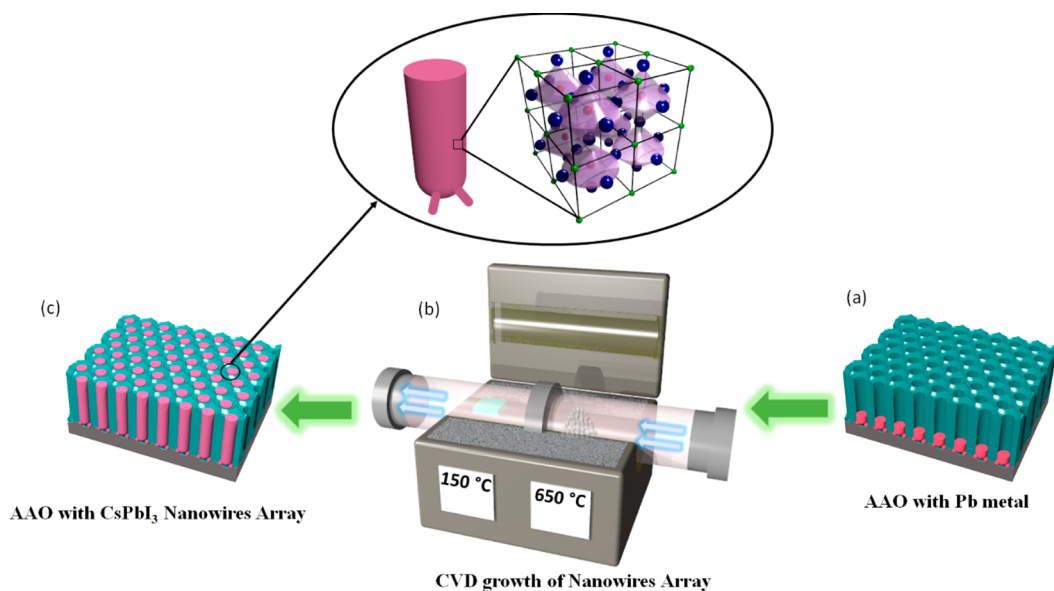
Figure 1. (a) AAM template with lead metal nanoclusters deposited in bottom of nanopores. (b) Growth schematic for cesium lead iodide perovskite NWs by chemical vapor diffusion of CsI with arrows showing transport direction of vapors. (c) The AAM sample after complete growth of cesium lead iodide NWs inside pores. (Top image is showing zoomed in crystal view of grown CsPbI$_3$ NW.)
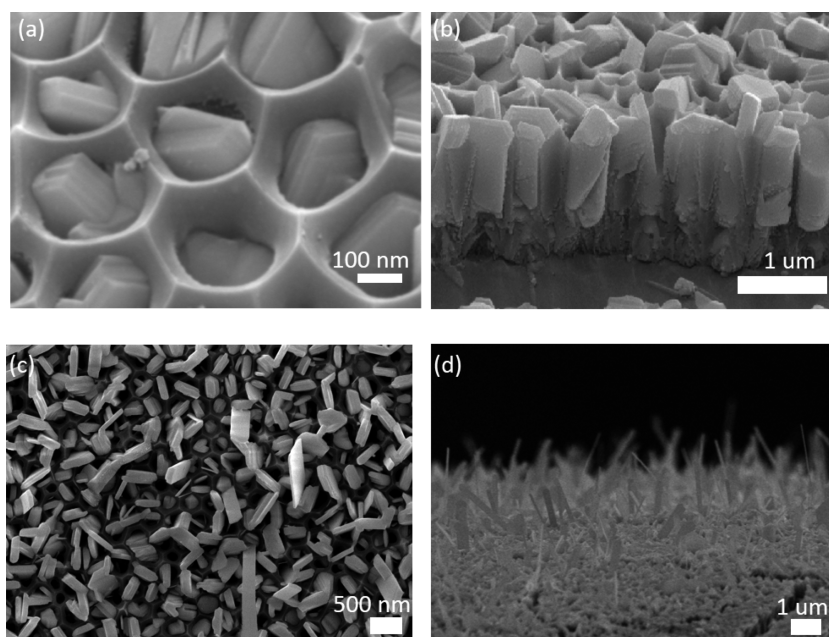

Figure 2. (a) Top SEM image of cesium lead iodide perovskite NWs inside AAM. (b) Cross-section SEM image of cesium lead iodide perovskite NWs inside AAM. (c) Top SEM image of cesium lead iodide perovskite nanowires coming out of AAM. (d) Cross-section SEM image of cesium lead iodide perovskite NWs coming out of AAM.

phase can be fabricated in nanoengineering templates, namely, anodic aluminum membranes (AAMs). The NWs were grown with a facile vapor growth method starting from Pb metal nanoclusters. Optical characterization of the as-grown NWs inside AAMs confirmed their stable cubic phase nature at room temperature. X-ray diffraction and transmission electron microscopy (TEM) study revealed that individual NWs are single crystalline with cubic phase. Excellent physical confinement and passivation of these NWs in AAM provide them extraordinary resistance against moisture that in turn helps in phase stabilization of CsPbI$_3$ NWs. Particularly, stability of these CsPbI$_3$ NWs was further tested inside organic polar

solvent, that is, isopropyl alcohol (IPA), and CsPbI$_3$ NWs were found stable inside IPA even after 30 days. Eventually, photodetector devices based on the NWs arrays was fabricated demonstrating reasonable performance.

The overall growth schematic for synthesis of CsPbI$_3$ NWs using a noncatalytic chemical vapor deposition (CVD) method is shown in Figure 1. There are several consecutive steps in this method explained in Methods in detail. Briefly, an aluminum chip was polished followed by multistep anodization in an acidic solution of phosphoric acid to form an AAM. Then lead metal was electrochemically deposited as precursor material in the bottom of AAM nanopores, as shown in Figure 1a.
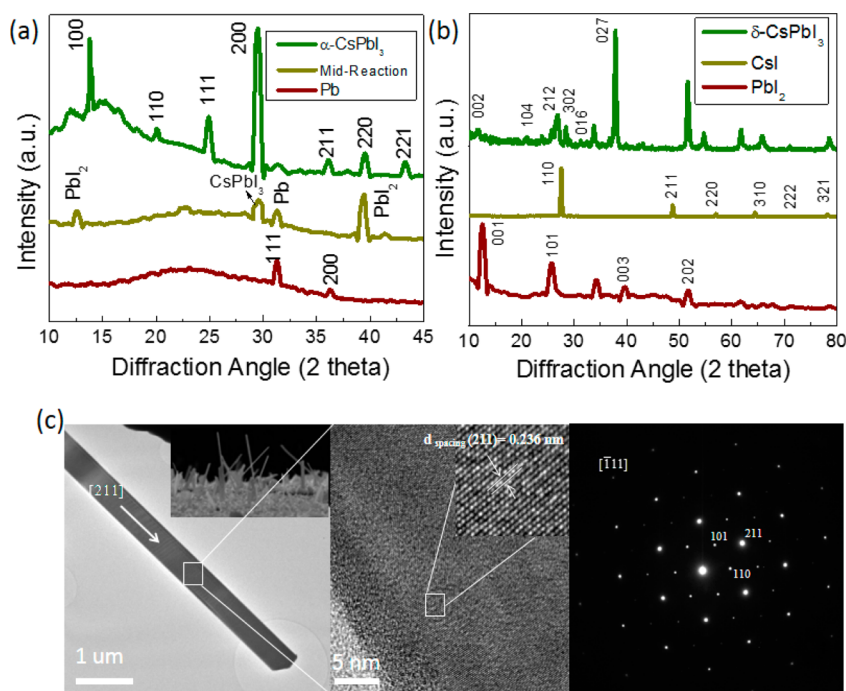
Figure 3. (a) X-ray diffraction peaks of Pb metal, short grown NWs (midphase) and CsPbI$_3$ NWs (after complete reaction) inside AAM. (b) X-ray diffraction peaks of thin film PbI$_2$, CsI, and CsPbI$_3$ on FTO glass. (c) TEM image (insert image is showing NWs sample with NWs coming outside of pores), HRTEM image of as fabricated CsPbI$_3$ NWs harvested onto TEM grid, and SAED image of CsPbI$_3$ NW.

Thereafter growth process of nanowires was performed inside the tube furnace in argon gas as an inert environment. The furnace involved in the growth process has two independent heating zones. AAM with lead metal clusters was placed inside the left heating zone with temperature setting of 150 °C and cesium iodide (CsI) powder was placed inside the right heating zone of furnace with temperature setting of 650 °C, as shown in Figure 1b. During growth, CsI was vaporized at elevated temperature and carried to the low-temperature zone by argon gas to initiate the growth process of CsPbI$_3$ NWs. After growth, CsPbI$_3$ NWs can be found inside AAM as schematically demonstrated in Figure 1c. Note that in the past perovskite NW growth was predominantly carried out with solution processes.[25−27] Although solution processes are easy to conduct, it is quite difficult to control the geometry of NWs, namely diameter, length, shape, and the arrangement of NWs in an array with solution process. Meanwhile, control over these parameters has both fundamental and practical significance. For instance, research has shown that optical properties of semiconducting NWs can be tuned by varying NW diameters and NW pitch in an array.[28−31] Also, for integrated electronic and optoelectronic device applications the geometric factors of NWs have to be well-defined due to high device packing density. Additionally, as the hybrid perovskite materials have stability issue, the NWs cannot survive lithographic device fabrication process that has been established for inorganic NWs. Therefore, using a nanoengineering template such as AAM to achieve NW growth and integration at the same time is highly preferential, considering the nature of AAM is electrically insulating, optically transparent, and chemically and mechanically robust.

Figure 2 shows scanning electron microscopy (SEM) images of the as-grown CsPbI$_3$ NWs inside an AAM. Figure 2a shows top SEM view of the grown NWs inside nanopores of an AAM. It is worth mentioning that the nanopore periodicity, diameter,

and length can be precisely controlled by tuning anodization and wet etching conditions (Methods).[32−34] The cross-sectional SEM image in Figure 2b demonstrates that the diameter of NWs, pitch of NWs array, and height of each NW are 200−250 nm, 500 nm, and ∼1 μm, respectively. It is also worth noting that if growth process was carried out for long time, NWs could grow vertically out of AAM nanopores, as shown in Figure 2c,d. Some of these overgrown NWs are as long as 10 μm as shown in Figure 2d. More interestingly, these NWs appear to be crystalline with preferred crystal orientation. To understand the property difference of these NWs inside AAM from bulk material of CsPbI$_3$, a CsPbI$_3$ thin film sample was fabricated on fluorine-doped tin oxide (FTO) glass by evaporation process (Methods). CsPbI$_3$ thin film was effectively fabricated by two-step evaporation of cesium iodide and lead iodide. The top view and cross-sectional view SEM images of this thin film perovskite sample is provided in Supporting Information (Figure S1). It can be visualized from SEM images that thin film sample is polycrystalline and it has no definite crystal orientations. To further investigate the quality and composition of these NWs, elemental mapping, and EDX were performed as provided in Supporting Information (Figure S2). It can be noted that elemental mix up of NW consists of Cs, Pb, and I. Trace of Al and O is also identified from AAM template.

To further investigate the crystalline nature of these grown NWs, X-ray diffraction (XRD) and TEM were performed. XRD patterns before and after growth of CsPbI$_3$ NWs inside AAM are provided in Figure 3a. The results show that the NW growth is a two-step process with PbI$_2$ as intermediate product before complete conversion to CsPbI$_3$. To verify this, XRD was performed for short time grown NWs (Supporting Information Figure S3). XRD peaks from Pb, PbI$_2$ and CsPbI$_3$ (as shown in Figure 3a midreaction XRD spectrum) were observed for short time grown NWs which is an unambiguous evidence that Pb metal is converted to PbI$_2$ before complete reaction to form
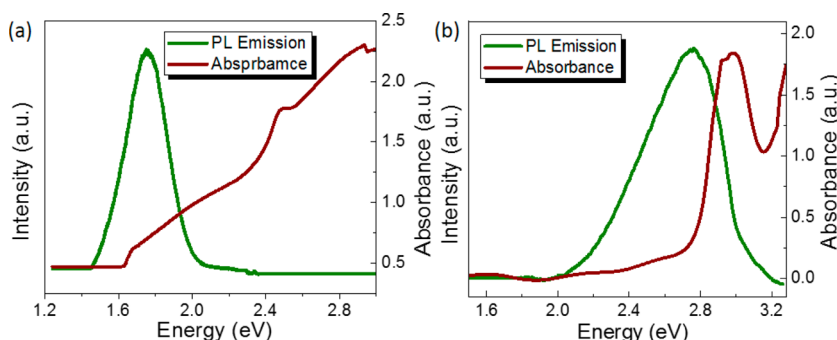
Figure 4. (a) Photoluminescence (PL) emission and absorbance curve from CsPbI₃ NWs inside AAM. (b) Photoluminescence (PL) emission and absorbance curve from thin film CsPbI₃ on FTO glass.

$CsPbI_3$. PbI_2 as intermediate product is akin to the growth of organic perovskite reported by us recently.[9,10,35,36] It is worth mentioning that XRD pattern of as-grown $CsPbI_3$ NWs match with cubic phase (α-$CsPbI_3$) as reported previously.[23,24] To compare the crystalline nature of $CsPbI_3$ NWs with thin films, XRD analysis was performed on $CsPbI_3$ thin film samples. XRD peaks obtained from $CsPbI_3$ thin films are shown in Figure 3b. XRD peaks from CsI and PbI_2 powder are also provided in Figure 3b. It is evident that the XRD patterns of the thin film match with that of orthorhombic phase (δ-$CsPbI_3$) $CsPbI_3$ reported previously.[21]

To further verify that the as-grown perovskite NWs are cubic in nature, high-resolution transmission electron microscopy (HRTEM) was employed. For this study, some of the NWs grown out of the AAM channels (inset image in Figure 3c) were transferred onto TEM grids with carbon mesh. Figure 3c shows TEM images and selective area electron diffraction (SAED) pattern of one of those NWs. As seen, SAED pattern indicates that the NW is highly crystalline with a zone axis of [$\bar{1}$11], which is matched with cubic structure of $CsPbI_3$ in terms of symmetry. High-resolution TEM image in Figure 3c shows the interplanar spacing of a $CsPbI_3$ NW is 0.236 nm that corresponds to the distance between two neighboring (211) planes of cubic $CsPbI_3$ NW. These planes have grown in the same direction of nanowire shown in Figure 3c and as a result, the growth direction of nanowire is identified as [211]. In addition, the indexed planes shown in SAED pattern together with our XRD result support the cubic structure of NWs.

After successful growth and crystal structure study of these grown NWs, their optical properties were investigated. Thin film $CsPbI_3$ optical properties were also studied at the same time for the sake of fair comparison. Figure 4a shows the photoluminescence (PL) emission and ultraviolet−visible (UV−vis) spectrum of $CsPbI_3$ NWs. For UV−vis measurement, 1 μm free-standing AAM sample embedded with NWs was attached on a glass substrate using UV curable epoxy. PL result shows a sharp emission excitonic peak at 1.74 eV that matches well with the cubic phase band gap of $CsPbI_3$ as reported in literature.[24,37,38] Absorbance curve from these NWs plotted in Figure 4a matches well with PL emission results and is consistent with previous reports on cubic phase $CsPbI_3$ as well. As aforementioned, $CsPbI_3$ NWs with band gap of 1.74 eV is a suitable candidate for many visible light optoelectronic applications. In fact, $CsPbI_3$ NWs with 1.74 eV band gap is particularly attractive to serve as the top cell in a tandem solar cell device structure with crystalline silicon with band gap of 1.1 eV serving as the bottom cell. Furthermore, optical constants and absorption constant of the grown NWs in AAM were

measured (Figure S4) by ellipsometry that provide data matching with ~1.7 eV band gap. It should be noted as well that the ellipsometry data in Figure S4 is for effective optical constants of the AAM/perovskite nanowire composite. Meanwhile, optical characterization was also performed on a thin film of $CsPbI_3$ as demonstrated in Figure 4b. It can be seen from PL emission peak and optical absorbance curve that thin film material band gap is 2.7 eV, indicating the orthorhombic phase of film.[21]

On the basis of the results from above structural and optical characterizations, it can be concluded that we have grown vertically aligned, high density stable cubic phase $CsPbI_3$ NWs inside AAMs. In contrast, as fabricated thin film $CsPbI_3$ are in orthorhombic phase at room temperature. The reasons of thin film crystallizing in orthorhombic phase are that bulk orthorhombic phase has higher internal energy and the orthorhombic phase is enthalpically favored at room temperature.[39,40] In addition, it was discovered that water/moisture plays an important role in catalyzing the transition process from black cubic phase to orthorhombic phase.[39] In our work, we attribute achievement of room temperature cubic $CsPbI_3$ NWs primarily to the following two reasons: (1) small dimensions of NWs increase surface area, high surface energy is reported to be helpful to stabilize the cubic phase;[23,24] (2) water molecules catalyze the transition from cubic phase to orthorhombic phase. However, in our work NWs are tightly embedded in AAM and well passivated by chemically and mechanically robust aluminum oxide material. This largely blocked the diffusion path of water molecules. In fact, our recently study has also revealed that protection against water and oxygen molecules provided by AAM can drastically improve the lifetime of $CH_3NH_3SnI_3$ NWs.[9] It is also worth noting that we have discovered that using CVD method is critical to achieve the cubic phase of the material. As shown in Supporting Information (Figure S5), $CsPbI_3$ NWs were also formed in AAM via spin coating of $CsPbI_3$ precursor solution at 2,000 rpm for 30 s. However, the crystalline structure was identified to be orthorhombic. This observation can be explained as such. During CVD growth, the cubic $CsPbI_3$ NWs were formed at the elevated temperature that can be maintained after cooling down to room temperature. However, spin coating was performed at room temperature, the as-grown NWs are in orthorhombic phase that is naturally stable at room temperature. Obviously, in our work an AAM is not only a nanoengineering template to guide $CsPbI_3$ NW growth but also a nanostructured packaging material to achieve stable cubic phase at room temperature for further optoelectronic applications. In fact, stability of these $CsPbI_3$ NWs was further
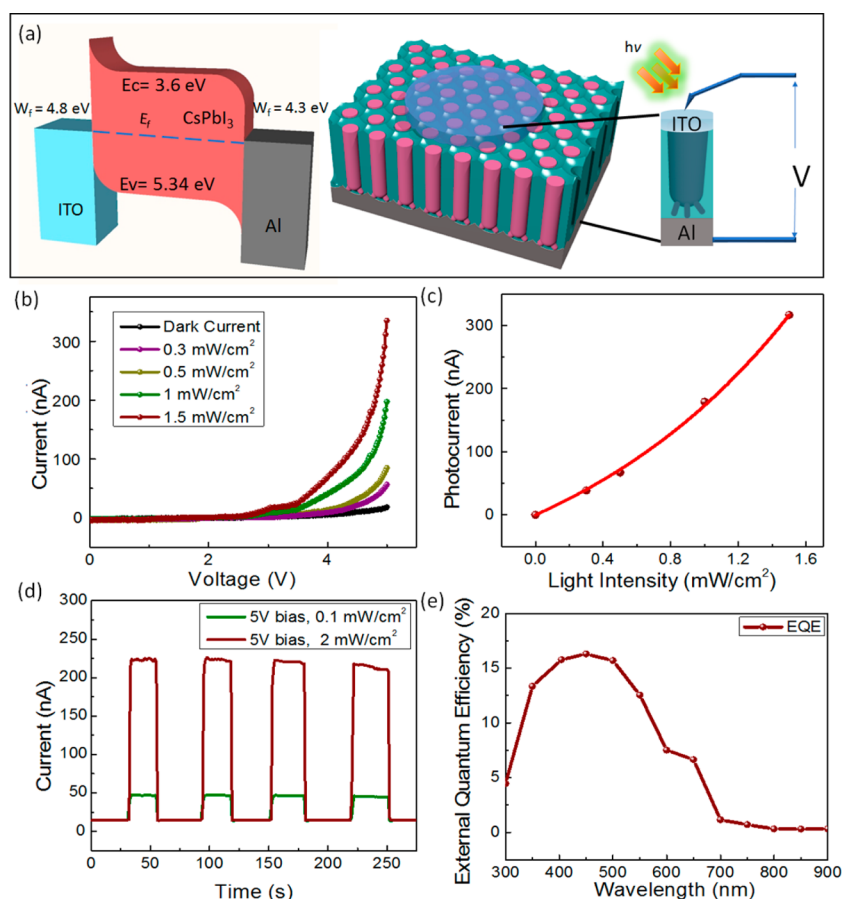
Figure 5. (a) Band diagram for CsPbI$_3$ perovskite NWs-based photodetector device with aluminum and ITO as electrodes, schematic for CsPbI$_3$ perovskite NWs based device with top circular electorode of ITO with area of 0.0314 cm^2. (b) Current−voltage curves for CsPbI$_3$ perovskite NWs device under different light intensities and 5 V bias. (c) Photocurrent response curve for CsPbI$_3$ perovskite NWs device. (d) Current variations with time for NWs device according to light switching at different time instants under different bias voltage. (e) External quantum efficiency (EQE) from CsPbI$_3$ NWs device inside AAM sample.

tested inside organic polar solvent, that is, IPA, and CsPbI$_3$ NWs were found stable inside IPA even after 30 days, as shown in Supporting Information (Figure S6).

The achieved CsPbI$_3$ NW with ∼1.7 eV band gap in this work is suitable for many optoelectronics devices, such as solar cells, photodetectors, and light-emitting diodes.[21,23,24] Particularly to demonstrate their application for photodetection, CsPbI$_3$ perovskite NWs embedded inside AAM were configured as photodetectors and their photoresponse was characterized. The device schematic is provided in Figure 5a, showing vertical NW array as the active component. The transparent top indium-doped tin oxide (ITO) layer with thickness of 250 nm was sputtered with circular area of 0.0314 cm^2 (Methods) while Al substrate serves as the bottom electrode. It is worth pointing out that this device configuration is highly advantageous for achieving high device integration density. Namely, the footprint of individual NWs is controlled by the AAM nanopore size, which is in the range of 100−500 nm. In fact, it is well-known that the nanopore pitch can be precisely controlled by the anodization voltage and the pore size and pitch can be as small as 10 nm.[41] This is attractive for constructing ultrahigh density electronic devices. Meanwhile for photonic and optoelectronic applications, NW pitch and diameter in the range of 100−500 nm is comparable to optical wavelength thus is sufficient. In our work, the pitch of the nanopores is 500 nm, corresponding to a NW density of ∼10^8

/cm^2. High NW density can be harnessed for fabricating high-resolution image sensors and recently we have reported NW array-based large scale image sensor.[10] Apart from favorable integration density, tunability of NW dimension, especially diameter, can lead to tunable optical property of NW arrays due to excitation of optical modes in NWs thus render devices with color selectivity.[28,31,42]

Figure 5a also shows the band diagram of the device. Here CsPbI$_3$ is regarded as an intrinsic semiconductor with work function around 4.47 eV.[43] Because of the work function difference with Al (4.3 eV) and ITO (4.8 eV), band bending is induced at the contact interface. Figure 5b shows I−V curves of CsPbI$_3$ perovskite NWs photodetector device obtained under different halogen light illumination intensities from 0.3 to 1.5 mW/cm^2. Note that an apparent turn on voltage can be observed on the I−V curves. This indicates existence of a contact energy barrier at the CsPbI$_3$/Al interface, which is mainly caused by the intrinsic nature of CsPbI$_3$ NW, as shown in the forward bias band diagram plotted in Supporting Information (Figure S7). The asymmetric metal contact causes schottky diode behavior from the device depicted in Figure 5a. Figure 5c demonstrates a superlinear increase of photocurrent with increasing light intensities, where photocurrent (I_{ph}) is calculated as the difference between light current (I_{light}) and dark current (I_{dark}).[44]

Photocurrent $(I_{ph}) = I_{light} - I_{dark}$

Figure 5d shows $I-t$ sampling plot of a photodetector under periodically switched light with a fixed bias and two different light intensities. Clearly the device is sensitive to light and showed quick photoresponse. Supporting Information Figure S8a shows that the photocurrent rise and decay time are 0.292 and 0.234 s (Supporting Information Figure S8a), respectively. For a photodetector device, responsivity and specific detectivity are also important figure-of-merits to quantify its performance and sensitivity. Here responsivity and specific detectivity for our device are provided in Supporting Information (Figure S8b). Specifically, responsivity reaches up to 6.7 mA/W with light intensity reaching to 1.5 mW/cm^2. Under light intensity of 1.5 mW/cm^2, specific detectivity was calculated to be 1.57×10^8 Jones. In addition to these measurements, external quantum efficiency (EQE) was also measured from these CsPbI$_3$ NWs based device using incident photon to current efficiency setup under 1 V bias. As shown in Figure 5e, EQE data plot indicates absorption cuts off at around 700 nm, which is consistent with our optical characterization measurements in Figure 4a. This fact also confirms that the CsPbI$_3$ NWs are in cubic black phase.

In this work, we demonstrate a vapor phase process to grow cesium lead iodide perovskite NWs inside AAM templates with high NW integration density. The structural characterization showed that individual NWs are single crystalline with high quality. Together with optical and electrical characterizations, the NWs were identified to be in stable cubic phase at room temperature. This intriguing fact is attributed to excellent passivation against invasion of water molecule as well as nanostructure associated high surface energy. To demonstrate device application of CsPbI$_3$ NWs, vertical NWs were configured as visible light photodetectors demonstrating reasonable performance. Overall, the discovery reported here suggests a novel and practical approach to stabilize the cubic phase of CsPbI$_3$ material, which will have broad applications for optoelectronics in the visible wavelength range.

■ METHODS

AAM Fabrication. Aluminum chips with size of 2 cm^2 were cut from aluminum foil (Alfa Aesar 99.9% purity) and sonicated in isopropyl alcohol for 10 min. Chips were then polished in polishing solution of 25 vol % HClO$_4$ and 75 vol % CH$_3$CH$_2$OH solution. Chips were then anodized twice in acidic solution of 200 mL H$_2$O/100 mL ethylene glycol/1 mL 85% H$_3$PO$_4$ under direct current voltage of 200 V followed by wet etching in 5 wt % phosphoric acid aqueous solution with heating at 53 °C.[9] After aluminum anodization, a thin barrier layer was formed at the bottom of nanopores. This thin barrier layer was reduced by a current ramping process reported earlier.[32]

Lead Electrodeposition. After fabrication of AAM, Pb metal was electrochemically deposited from aqueous solution of lead chloride. An aqueous solution was prepared by adding 70 g of lead chloride and 42 g of trisodium citrate in 1000 mL of water. Electrochemical deposition was performed by applying a sinousaidal signal with 6.5 V and 50 Hz frequency. Uniform and ductile lead metal was found deposited in the bottom of nanopores of AAM as depicted in Figure S3a.

Cesium Lead Iodide Perovskite NWs and Device Fabrication. For fabrication of CsPbI$_3$ NWs inside AAM, a tube furnance with two zones (temperature programmable

independetly) was used. Commercial CsI powder (Sigma-Aldrich) was placed in one heating zone with temperature set at 650 °C while the AAM with Pb metal was placed in the other heating zone downstream with temperature set at 150 °C as demonstrated in Figure 1b. The reaction was carried out for 10 h with distance between source powder and substrate at 20 cm. Vapor of CsI was transported to other side by using argon as carrier gas. Upon successful fabrication of perovskite NWs, top surface of CsPbI$_3$ was cleaned by ion milling at 250 V with 80° angle for 1 h time. After ion milling of top surface, photodetector device was fabricated by direct current sputtering of 250 nm thick ITO on top inside a vacuum chamber using ITO target with circular mask of 0.0314 cm^2 area.

Fabrication of Cesium Lead Iodide Perovskite Thin Film and Device. Flourine-doped tin oxide (FTO) glass (Hartford Glass CO. Inc.) was first cleaned by sonication inside acetone, isopropyl alcohol, and deionized water, respectively.[45] Then a two-step thermal evaporation was performed on FTO glass by deposition of PbI$_2$ (Purity 99%, Sigma-Aldrich) and CsI in order at a deposition rate of 1.5 Å/s. Source powder was placed in different tungsten crucibles and deposition was performed one by one without breaking the vacuum (pressure of 4×10^{-4} pa). The final sample thickness was around 500 nm as shown in Supporting Information Figure S1.

Chracterization. *Scanning Electron Microscopy.* Cross-sectional and top SEM images of AAM and thin film samples were obtained by using field emission scanning electron micrscopy JEOL JSM-7100F in back scattered electron (BSE) mode.

X-ray Diffraction and TEM Image. Crystalline studies of material was performed by Bruker D8 X-ray diffracttometer. Transmission electron microscopy image and SAED pattern for morphology of NWs was studied by using JEOL (2010F) under an accelerating voltage of 200 V.

PL and Absorbance Spectrum. PL emission spectrum and were obtained from FLS920P flourescence spectrometer. Absorbance wavelengths spectrum for NWs and thin film sample was obtained from Varian Cary 500 spectrometer (Varian, U.S.A.) and FLS920P flourescence spectrometer with a scanning rate of 240 nm/min.

Complex Optical Constants n and k. J.A. Woollam Co. M2000X-FB-300XTF elipsometer was used to record optical constants.

QE Measurement. Quantum efficiency was recorded versus wavelength under white light bias of nearly 5 mW/cm^2 using Oriel QE−PV-SI(Newport Connection).

Device Chracterization. Chracterization of device using $I-V$ and $I-t$ curves was performed by HP 4156A Analyzer along with probe station (Signatone, U.S.A.) and broadband Halogen lamp (light intensities control option).

■ ASSOCIATED CONTENT

Ⓢ Supporting Information

The Supporting Information is available free of charge on the ACS Publications website at DOI: 10.1021/acs.nano-lett.7b02101.

Figures S1−S8 are available (PDF)

■ AUTHOR INFORMATION

Corresponding Author
*E-mail: eezfan@ust.hk.

ORCID ⊙

Aashir Waleed: 0000-0002-6929-8373
Mohammad Mahdi Tavakoli: 0000-0002-8393-6028
Zhiyong Fan: 0000-0002-5397-0129

Notes
The authors declare no competing financial interest.

■ REFERENCES

(1) Dong, Q.; Fang, Y.; Shao, Y.; Mulligan, P.; Qiu, J.; Cao, L.; Huang, J. *Science* **2015**, *347* (6225), 967−970.

(2) Stranks, S. D.; Eperon, G. E.; Grancini, G.; Menelaou, C.; Alcocer, M. J. P.; Leijtens, T.; Herz, L. M.; Petrozza, A.; Snaith, H. J. *Science* **2013**, *342* (6156), 341−344.

(3) Xing, G.; Mathews, N.; Sun, S.; Lim, S. S.; Lam, Y. M.; Grätzel, M.; Mhaisalkar, S.; Sum, T. C. *Science* **2013**, *342* (6156), 344−347.

(4) Nie, W.; Tsai, H.; Asadpour, R.; Blancon, J.-C.; Neukirch, A. J.; Gupta, G.; Crochet, J. J.; Chhowalla, M.; Tretiak, S.; Alam, M. A.; Wang, H.-L.; Mohite, A. D. *Science* **2015**, *347* (6221), 522−525.

(5) Tavakoli, M. M.; Tavakoli, R.; Nourbakhsh, Z.; Waleed, A.; Virk, U. S.; Fan, Z. *Adv. Mater. Interfaces* **2016**, *3* (11), 1500790.

(6) Tavakoli, M. M.; Tsui, K.-H.; Zhang, Q.; He, J.; Yao, Y.; Li, D.; Fan, Z. *ACS Nano* **2015**, *9* (10), 10287−10295.

(7) Park, N.-G. *Inorg. Chem.* **2017**, *56* (1), 3−10.

(8) Lu, H.; Tian, W.; Cao, F.; Ma, Y.; Gu, B.; Li, L. *Adv. Funct. Mater.* **2016**, *26* (8), 1296−1302.

(9) Waleed, A.; Tavakoli, M. M.; Gu, L.; Wang, Z.; Zhang, D.; Manikandan, A.; Zhang, Q.; Zhang, R.; Chueh, Y.-L.; Fan, Z. *Nano Lett.* **2017**, *17* (1), 523−530.

(10) Gu, L.; Tavakoli, M. M.; Zhang, D.; Zhang, Q.; Waleed, A.; Xiao, Y.; Tsui, K.-H.; Lin, Y.; Liao, L.; Wang, J.; Fan, Z. *Adv. Mater.* **2016**, *28* (44), 9713−9721.

(11) Niu, G.; Guo, X.; Wang, L. *J. Mater. Chem. A* **2015**, *3* (17), 8970−8980.

(12) Juarez-Perez, E. J.; Hawash, Z.; Raga, S. R.; Ono, L. K.; Qi, Y. *Energy Environ. Sci.* **2016**, *9* (11), 3406−3410.

(13) Fu, Y.; Zhu, H.; Stoumpos, C. C.; Ding, Q.; Wang, J.; Kanatzidis, M. G.; Zhu, X.; Jin, S. *ACS Nano* **2016**, *10* (8), 7963−7972.

(14) Ramasamy, P.; Lim, D.-H.; Kim, B.; Lee, S.-H.; Lee, M.-S.; Lee, J.-S. *Chem. Commun.* **2016**, *52* (10), 2067−2070.

(15) Luo, P.; Xia, W.; Zhou, S.; Sun, L.; Cheng, J.; Xu, C.; Lu, Y. *J. Phys. Chem. Lett.* **2016**, *7* (18), 3603−3608.

(16) Chen, J.; Fu, Y.; Samad, L.; Dang, L.; Zhao, Y.; Shen, S.; Guo, L.; Jin, S. *Nano Lett.* **2017**, *17* (1), 460−466.

(17) Song, J.; Li, J.; Li, X.; Xu, L.; Dong, Y.; Zeng, H. *Adv. Mater.* **2015**, *27* (44), 7162−7167.

(18) Su, R.; Diederichs, C.; Wang, J.; Liew, T. C. H.; Zhao, J.; Liu, S.; Xu, W.; Chen, Z.; Xiong, Q. *Nano Lett.* **2017**, *17* (6), 3982−3988.

(19) Beal, R. E.; Slotcavage, D. J.; Leijtens, T.; Bowring, A. R.; Belisle, R. A.; Nguyen, W. H.; Burkhard, G. F.; Hoke, E. T.; McGehee, M. D. *J. Phys. Chem. Lett.* **2016**, *7* (5), 746−751.

(20) Sharma, S.; Weiden, N.; Weiss, A. Phase Diagrams of Quasibinary Systems of the Type: ABX3 — A′BX3; ABX3 — AB′X3, and ABX3 — ABX′3; X = Halogen. *Z. Phys. Chem.* **1992**, *175*, 63.

(21) Eperon, G. E.; Paterno, G. M.; Sutton, R. J.; Zampetti, A.; Haghighirad, A. A.; Cacialli, F.; Snaith, H. J. *J. Mater. Chem. A* **2015**, *3* (39), 19688−19695.

(22) Dastidar, S.; Egger, D. A.; Tan, L. Z.; Cromer, S. B.; Dillon, A. D.; Liu, S.; Kronik, L.; Rappe, A. M.; Fafarman, A. T. *Nano Lett.* **2016**, *16* (6), 3563−3570.

(23) Protesescu, L.; Yakunin, S.; Bodnarchuk, M. I.; Krieg, F.; Caputo, R.; Hendon, C. H.; Yang, R. X.; Walsh, A.; Kovalenko, M. V. *Nano Lett.* **2015**, *15* (6), 3692−3696.

(24) Swarnkar, A.; Marshall, A. R.; Sanehira, E. M.; Chernomordik, B. D.; Moore, D. T.; Christians, J. A.; Chakrabarti, T.; Luther, J. M. *Science* **2016**, *354* (6308), 92−95.

(25) Zhang, D.; Eaton, S. W.; Yu, Y.; Dou, L.; Yang, P. *J. Am. Chem. Soc.* **2015**, *137* (29), 9230−9233.

(26) Fu, Y.; Meng, F.; Rowley, M. B.; Thompson, B. J.; Shearer, M. J.; Ma, D.; Hamers, R. J.; Wright, J. C.; Jin, S. *J. Am. Chem. Soc.* **2015**, *137* (17), 5810−5818.

(27) Dong, D.; Deng, H.; Hu, C.; Song, H.; Qiao, K.; Yang, X.; Zhang, J.; Cai, F.; Tang, J.; Song, H. *Nanoscale* **2017**, *9* (4), 1567−1574.

(28) Chueh, Y.-L.; Fan, Z.; Takei, K.; Ko, H.; Kapadia, R.; Rathore, A. A.; Miller, N.; Yu, K.; Wu, M.; Haller, E. E.; Javey, A. *Nano Lett.* **2010**, *10* (2), 520−523.

(29) Hua, B.; Wang, B.; Yu, M.; Leu, P. W.; Fan, Z. *Nano Energy* **2013**, *2* (5), 951−957.

(30) Yu, R.; Lin, Q.; Leung, S.-F.; Fan, Z. *Nano Energy* **2012**, *1* (1), 57−72.

(31) Park, H.; Dan, Y.; Seo, K.; Yu, Y. J.; Duane, P. K.; Wober, M.; Crozier, K. B. *Nano Lett.* **2014**, *14* (4), 1804−1809.

(32) Fan, Z.; Razavi, H.; Do, J.-w.; Moriwaki, A.; Ergen, O.; Chueh, Y.-L.; Leu, P. W.; Ho, J. C.; Takahashi, T.; Reichertz, L. A.; Neale, S.; Yu, K.; Wu, M.; Ager, J. W.; Javey, A. *Nat. Mater.* **2009**, *8* (8), 648−653.

(33) Leung, S.-F.; Yu, M.; Lin, Q.; Kwon, K.; Ching, K.-L.; Gu, L.; Yu, K.; Fan, Z. *Nano Lett.* **2012**, *12* (7), 3682−3689.

(34) Hussain, S.; Hussain, S.; Waleed, A.; Tavakoli, M. M.; Wang, Z.; Yang, S.; Fan, Z.; Nadeem, M. A. *ACS Appl. Mater. Interfaces* **2016**, *8* (51), 35315−35322.

(35) Waleed, A.; Fan, Z. *Sci. Bull.* **2017**, *62* (9), 645−647.

(36) Tavakoli, M. M.; Waleed, A.; Gu, L.; Zhang, D.; Tavakoli, R.; Lei, B.; Su, W.; Fang, F.; Fan, Z. *Nanoscale* **2017**, *9* (18), 5828−5834.

(37) Park, K.; Lee, J. W.; Kim, J. D.; Han, N. S.; Jang, D. M.; Jeong, S.; Park, J.; Song, J. K. *J. Phys. Chem. Lett.* **2016**, *7* (18), 3703−3710.

(38) Zhang, Q.; Su, R.; Liu, X.; Xing, J.; Sum, T. C.; Xiong, Q. *Adv. Funct. Mater.* **2016**, *26* (34), 6238−6245.

(39) Dastidar, S.; Hawley, C. J.; Dillon, A. D.; Gutierrez-Perez, A. D.; Spanier, J. E.; Fafarman, A. T. *J. Phys. Chem. Lett.* **2017**, *8* (6), 1278−1282.

(40) Nedelcu, G.; Protesescu, L.; Yakunin, S.; Bodnarchuk, M. I.; Grotevent, M. J.; Kovalenko, M. V. *Nano Lett.* **2015**, *15* (8), 5635−5640.

(41) Bruggemann, D. *J. Nanomater.* **2013**, *2013*, 18.

(42) Lin, Q.; Hua, B.; Leung, S.-f.; Duan, X.; Fan, Z. *ACS Nano* **2013**, *7* (3), 2725−2732.

(43) Li, G.; Rivarola, F. W. R.; Davis, N. J. L. K.; Bai, S.; Jellicoe, T. C.; de la Peña, F.; Hou, S.; Ducati, C.; Gao, F.; Friend, R. H.; Greenham, N. C.; Tan, Z.-K. *Adv. Mater.* **2016**, *28* (18), 3528−3534.

(44) Liu, X.; Gu, L.; Zhang, Q.; Wu, J.; Long, Y.; Fan, Z. *Nat. Commun.* **2014**, *5*, 4007.

(45) Waleed, A.; Zhang, Q.; Tavakoli, M. M.; Leung, S.-F.; Gu, L.; He, J.; Mo, X.; Fan, Z. *Sci. Bull.* **2016**, *61* (1), 86−91.